THE JOURNAL OF BIOLOGICAL CHEMISTRY VOL. 290, NO. 47, pp. 28097–28106, November 20, 2015
Published in the U.S.A.

Ablation of the Ferroptosis Inhibitor Glutathione Peroxidase 4 in Neurons Results in Rapid Motor Neuron Degeneration and Paralysis*

Received for publication, July 20, 2015, and in revised form, September 22, 2015 Published, JBC Papers in Press, September 23, 2015, DOI 10.1074/jbc.M115.680090

Liuji Chen[‡], **William Sealy Hambright**[‡], **Ren Na**[‡], **and Qitao Ran**[‡§1]

From the [‡]*Department of Cellular and Structural Biology, University of Texas Health Science Center at San Antonio, San Antonio, Texas 78229 and the* [§]*Research Service, South Texas Veterans Health Care System, San Antonio, Texas 78229*

Background: Glutathione peroxidase 4 (GPX4) is shown to be a key inhibitor of ferroptosis, a cell death mechanism involving lipid reactive oxygen species.
Results: Conditional ablation of *Gpx4* in neurons resulted in rapid motor neuron degeneration and paralysis in mice.
Conclusion: Lack of GPX4 triggered motor neuron degeneration characterized by ferroptosis.
Significance: Ferroptosis inhibition may be essential for motor neuron health and survival *in vivo*.

Glutathione peroxidase 4 (GPX4), an antioxidant defense enzyme active in repairing oxidative damage to lipids, is a key inhibitor of ferroptosis, a non-apoptotic form of cell death involving lipid reactive oxygen species. Here we show that GPX4 is essential for motor neuron health and survival *in vivo*. Conditional ablation of *Gpx4* in neurons of adult mice resulted in rapid onset and progression of paralysis and death. Pathological inspection revealed that the paralyzed mice had a dramatic degeneration of motor neurons in the spinal cord but had no overt neuron degeneration in the cerebral cortex. Consistent with the role of GPX4 as a ferroptosis inhibitor, spinal motor neuron degeneration induced by *Gpx4* ablation exhibited features of ferroptosis, including no caspase-3 activation, no TUNEL staining, activation of ERKs, and elevated spinal inflammation. Supplementation with vitamin E, another inhibitor of ferroptosis, delayed the onset of paralysis and death induced by *Gpx4* ablation. Also, lipid peroxidation and mitochondrial dysfunction appeared to be involved in ferroptosis of motor neurons induced by *Gpx4* ablation. Taken together, the dramatic motor neuron degeneration and paralysis induced by *Gpx4* ablation suggest that ferroptosis inhibition by GPX4 is essential for motor neuron health and survival *in vivo*.

Glutathione peroxidase 4 (GPX4) is a selenoprotein glutathione peroxidase with pleotropic functions (1). In somatic cells, GPX4 is important in the protection against lipid peroxidation because of its ability to reduce hydroperoxides in lipids such as phospholipids, cholesterol, and cholesterol ester (1). GPX4 has been shown previously to suppress apoptosis (2–4). However, Yang *et al.* (5, 6) recently identified GPX4 as a key inhibitor of ferroptosis, an oxidative, iron-dependent type of cell death that exhibits features different from other cell death mechanisms, and ferroptosis-inducing compounds were shown to inhibit GPX4 enzyme activity directly by binding to GPX4 protein (*e.g.* RSL3) or indirectly by depleting glutathione (*e.g.* erastin) (7).

Previous studies indicate that GPX4 is essential for embryonic development (8, 9) as well as for health maintenance in adult animals (10). In this study, to investigate the importance of GPX4 in the neuron health of adult animals, we generated a *Gpx4* neuronal inducible knockout (Gpx4NIKO)[2] mouse in which ablation of *Gpx4* in neurons can be achieved by tamoxifen (TAM) treatment. Our results indicated that, after TAM treatment, Gpx4NIKO mice became rapidly paralyzed, exhibited severe muscle atrophy, and died within 8 days. Pathological inspection indicated that *Gpx4* ablation led to a dramatic degeneration of motor neurons in the spinal cord but had no overt effect on neurons in the cerebral cortex. The specific vulnerability of spinal motor neurons to GPX4 deficiency was corroborated by the mild phenotype observed in another mouse model with *Gpx4* ablation in cortical neurons. Consistent with the role of GPX4 as a ferroptosis inhibitor, spinal motor neuron degeneration induced by *Gpx4* ablation is characterized by ferroptosis. The robust motor neuron degeneration induced by *Gpx4* ablation suggests that ferroptosis inhibition is essential for motor neuron health and survival *in vivo*.

Experimental Procedures

Animals and Procedures—The generation of Gpx4(f/f) mice has been described previously (10). The Slick H mice and Camk2α-creERT mice were obtained from The Jackson Laboratories (Bar Harbor, ME). Gpx4NIKO (Gpx4(f/f);Slick) mice were generated by two-step cross-breeding between Gpx4(f/f) mice with Slick H mice. Gpx4NIKO mice were subsequently

* The authors declare that they have no conflicts of interest with the contents of this article.

[1] Supported by a merit review grant from the Department of Veterans Affairs, a grant from the Alzheimer's Association, and an award from The William and Ella Owens Medical Research Foundation. To whom correspondence should be addressed: Dept. of Cellular and Structural Biology, University of Texas Health Science Center at San Antonio, 7703 Floyd Curl Dr., San Antonio, TX 78229. Tel.: 210-567-3842; Fax: 210-567-6781; E-mail: ran@uthscsa.edu.

[2] The abbreviations used are: NIKO, neuronal inducible knockout; TAM, tamoxifen; 4-HNE, 4-hydroxynonenal; Slick H, single-neuron labeling with inducible Cre-mediated knockout, H line; creERT, Cre recombinase fused to a mutated ligand-binding domain of the human estrogen receptor; ChAT, choline acetyltransferase; Syn, synaptophysin.

cross-bred with Gpx4(f/f) mice to generate Gpx4NIKO mice and control Gpx4(f/f) mice used in this study. Gpx4(f/f); Camk2α-creERT mice were obtained by two-step cross-breeding between Gpx4(f/f) mice and Camk2α-creERT mice.

Tamoxifen (T5648, Sigma) was dissolved in corn oil at a concentration of 10 mg/ml. Tamoxifen was administered to mice intraperitoneally at a dose of 60 mg/kg for a total of five injections (once daily). The vitamin E-enriched diet was formulated and manufactured by Bio-Serv (Frenchtown, NJ). The diet was on the basis of the standard rodent diet AIN-93G but had 1000 IU/kg vitamin E. The standard chow diet used had 150 IU/kg vitamin E. All animal procedures in this study were reviewed and approved by the Institutional Animal Care and Use Committees of the University of Texas Health Science Center at San Antonio and the Audie Murphy Memorial Veterans Hospital, South Texas Veterans Health Care System.

Locomotor Function Assay—Rotarod performance was measured with a Rotamex 4/8 (Columbus Instruments, Columbus, OH) using an accelerating rod protocol. The initial speed of the rod was set to 2 rpm with a linear acceleration to 40 rpm over 300 s. The latencies to fall were used as indicators of rotarod performance.

Survival Determination—Mice were checked twice daily for general appearance and locomotor behavior, including movement initiation, walking, and turning. When onset of paralysis (stiffness of hind limbs that led to awkwardness in walking and maintaining balance) occurred, food pellets were supplied on the cage floor for easy access, and the water bottle was lowered to ensure water access without standing on the hind limbs. A mouse that were immobile for a period of 30 s because of paralysis in four limbs would be euthanized humanly.

Detection of Ablation of the Gpx4 Gene—A PCR-based method was used to detect the recombination of the floxed *Gpx4* gene allele. As shown in Fig. 2*A*, using a pair of primers (P1, 5′-TAC TGC AAC AGC TCC GAG TTC-3′; P2, 5′-CTT CAC CAC GCA GCC GTT CT-3′) flanking the floxed *Gpx4* region between exon 2 (E2) and exon 4 (E4), the size of the amplicon derived from the recombined *Gpx4* allele (rGpx4) was 700 bp.

Tissue Preparation and Immunofluorescence Staining—Mice were anesthetized and perfused transcardially, first with saline and then with 4% para-formaldehyde. Perfused spines were collected, post-fixed in 4% paraformaldehyde at 4 °C overnight, decalcified in 10% EDTA (pH 7.4) for a week, and equilibrated in 30% sucrose in PBS for 1–2 days at 4 °C. The spines were then frozen by submersion in 2-metylbutane chilled in dry ice. Spine sections at a thickness of 16 μm were made using a cryostat.

For immunofluorescence staining, spinal cord sections were blocked with blocking buffer (1% horse serum in PBS and 0.3% Triton X-100) for 30 min and then incubated with primary antibody in PBS at 4 °C overnight. The sections were then washed three times with PBS and incubated with fluorophore-conjugated secondary antibody in PBS for 1 h at room temperature. After washing three times, slides were mounted with ProLong Gold antifade reagent (catalog no. P36930, Invitrogen).

TUNEL Staining—TUNEL labeling was performed using the TACS® TdT *in situ* fluorescein kit (R&D System, Minneapolis, MN). Sections treated with TACS nuclease to generate DNA breaks were used as a positive control.

Antibodies and Western Blotting—The antibodies used were as follows: anti-NeuN (catalog no. MAB377, Millipore, Billerica, MA); anti-synaptophysin, anti-glial fibrillary acidic protein (GFAP), anti-ChAT, anti-PSD95, anti-caspase-3, anti-actin, anti-total ERK1/2, and anti-phospho-ERK1/2 (Cell Signaling Technology, Beverly, MA); anti-Iba-1 (Invitrogen); anti-4-HNE (R&D Systems); and anti-GPX4 (generated in-house).

Immunoblotting was performed as described previously (11). Briefly, tissues were homogenized in radioimmune precipitation assay buffer (20 mM Tris (pH 7.4), 0.25 M NaCl, 1 mM EDTA, 0.5% Nonidet P-40, and 50 mM sodium fluoride) supplemented with protease inhibitors. Equal amounts of total proteins (20 μg) were separated by 4–20% SDS-PAGE and transferred to nitrocellulose membranes. The membranes were blocked for 1 h in 5% nonfat dry milk and incubated for 2 h at room temperature with the primary antibody. After washing, the membranes were incubated further with an HRP-conjugated secondary antibody. The bands were visualized using an ECL Kit (catalog no. RPN2132, GE Healthcare). The bands were quantified using National Institutes of Health ImageJ software and normalized to the loading control (Actin). The mean level of the protein of interest (the ratio of protein to Actin) in controls was arbitrarily assigned as 1, and relative data were expressed as mean ± S.E.

Electron Transport Chain Complex IV and Complex I Activity—The activities of complex IV and I in spinal cord tissues were determined using the complex IV mouse enzyme activity microplate assay kit and the complex I enzyme activity microplate assay kit (MitoSciences, Eugene, OR), respectively. Briefly, tissue samples were prepared, and complex IV and complex I enzymes were extracted and immunocaptured within the wells of the microplate using protocols provided by the manufacturer. The activity of complex IV was determined colorimetrically by following the oxidation of reduced cytochrome *c* as an absorbance decrease at 550 nm. The activity of complex IV was expressed as mA_{550}/min (where m*A* is milliAbsorbance). The activity of complex I enzyme was determined by following the oxidation of NADH to NAD^+ and the simultaneous reduction of a dye, which leads to increased absorbance at 450 nm. The activity of complex I was expressed as mA_{450}/min.

Statistics—Data are expressed as mean ± S.E. Results were analyzed statistically using two-way analysis of variance or Student's *t* test when appropriate. Statistical significance was set to a minimum of $p < 0.05$.

Results

Paralysis, Muscle Atrophy, and Death of Gpx4NIKO Mice Induced by TAM Treatment to Ablate Gpx4—We were interested in determining the importance of GPX4 in the neuron health of adult animals. We previously generated Gpx4(f/f) mice, a mouse model with floxed *Gpx4* alleles (10). To generate a conditional neuron-specific *Gpx4* knockout mouse, we cross-bred Gpx4(f/f) mice with single-neuron labeling with inducible Cre-mediated knockout, H line (Slick H) mice, which have a Slick transgene that expresses Cre recombinase fused to a

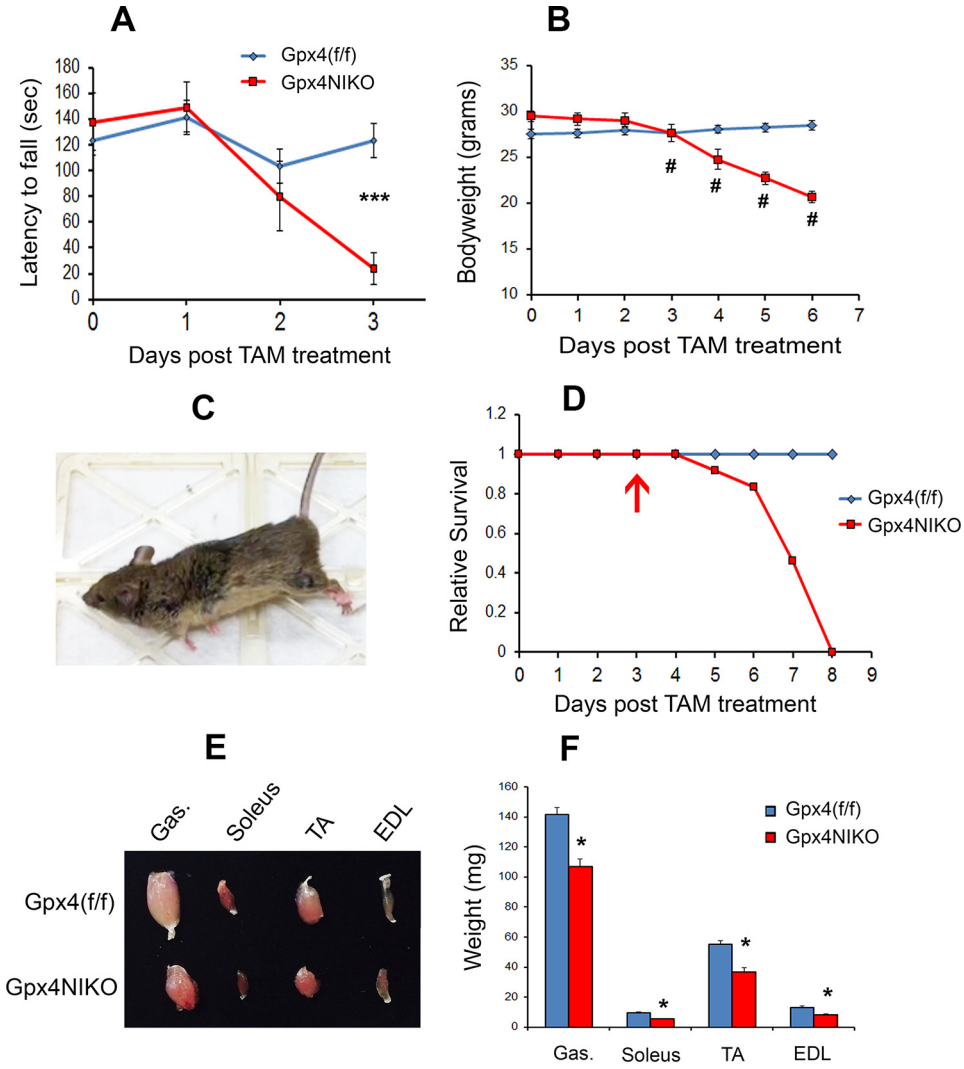

FIGURE 1. ***Gpx4* ablation induced rapid paralysis, muscle atrophy, and death in Gpx4NIKO mice, a mouse model with inducible ablation of *Gpx4* in neurons.** *A*, rotarod performance of Gpx4NIKO mice ($n = 7$, male and female) and Gpx4(f/f) mice ($n = 7$, male and female) after TAM treatment. ***, $p < 0.001$. *B*, body weights of Gpx4NIKO mice ($n = 8$, male) and Gpx4(f/f) mice ($n = 11$, male) after TAM treatment. #, $p < 0.01$. *C*, a paralyzed Gpx4NIKO mouse on day 6 post-TAM treatment. *D*, survival curves of Gpx4NIKO mice ($n = 24$, male and female) and Gpx4(f/f) mice ($n = 16$, male and female) after TAM treatment. The *arrow* indicates onset of paralysis. *E*, individual hind limb muscles (gastrocnemius (*Gas*), extensor digitorum longus (*EDL*), soleus, and tibialis anterior (*TA*)) from a Gpx4NIKO mouse and a Gpx4(f/f) mouse on day 6 post-TAM treatment. *F*, hind limb muscle weights on day 6 post-treatment ($n = 5$, male). *: $p < 0.05$.

mutated ligand-binding domain of the human estrogen receptor (creERT) and YFP/GFP in neurons (12, 13), and obtained mice with two floxed *Gpx4* alleles and the Slick transgene (Gpx4(f/f);Slick). We called these mice Gpx4NIKO mice.

Interestingly, TAM treatment to ablate *Gpx4* in adult Gpx4NIKO mice (3–4 months of age) resulted in a striking paralysis phenotype. On day 3 post-TAM treatment, all Gpx4NIKO mice showed stiffness of hind limbs, which signaled the onset of paralysis. The stiffness of the hind limbs led to awkwardness in walking and difficulty in maintaining balance. In a rotarod task that measures locomotor function, Gpx4NIKO mice had a significantly decreased latency time compared with Gpx4(f/f) mice on day 3, indicating loss of locomotor coordination ability (Fig. 1*A*). The mice also showed a significant loss of body weight from the previous day, starting on day 3 (Fig. 1*B*). After the onset of paralysis, Gpx4NIKO mice quickly progressed to loss of use of the hind limbs and became paralyzed in the lower body (Fig. 1*C*, also shown in supplemental Movie 1). Death started to occur on day 5. As shown by the survival curves in Fig. 1*D*, all Gpx4NIKO mice were dead within 8 days post-TAM treatment. Correlating with paralysis development was severe atrophy of hind limb muscles in these mice. Pictures of individual hind limb muscles from a control Gpx4(f/f) mouse and a Gpx4NIKO mouse at day 6 post-TAM treatment are presented in Fig. 1*E*, and the muscle weight data from these two groups of mice are presented in Fig. 1*F*. These data demonstrate that Gpx4NIKO mice had a significant loss of muscle mass. The paralysis, muscle atrophy, and death phenotypes induced by TAM treatment were subsequently duplicated in a second cohort of Gpx4NIKO mice.

A Dramatic Degeneration of Motor Neurons in the Spinal Cords of the Paralyzed Gpx4NIKO Mice—To investigate the cause of paralysis in Gpx4NIKO mice, we first sought to verify the extent of *Gpx4* ablation in TAM-treated Gpx4NIKO mice. Using a PCR-based method designed to detect the recombination of the floxed *Gpx4* alleles, we examined the ablation of

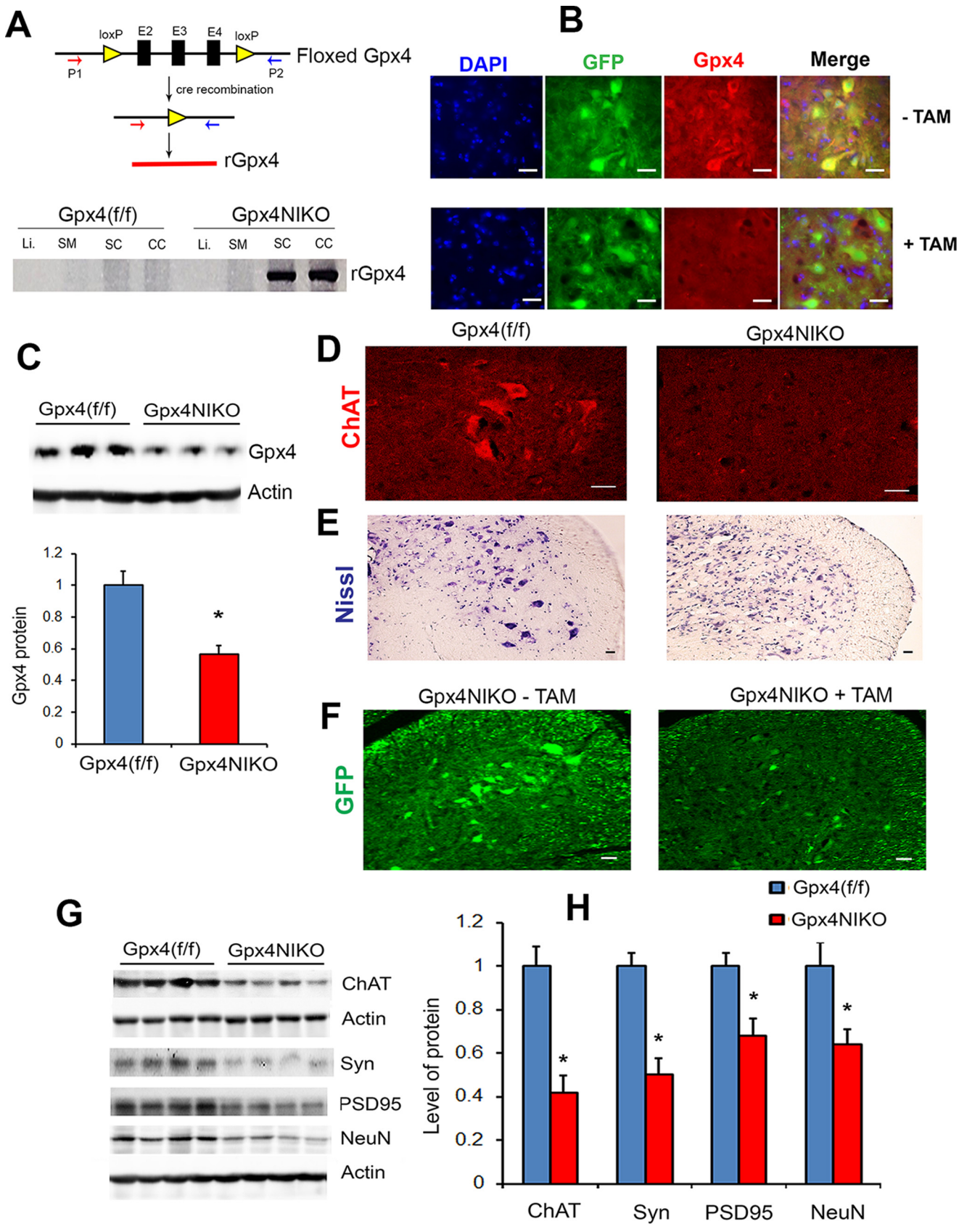
A
loxP
E2
E3
E4
loxP
Floxed Gpx4
P1
P2
cre recombination
rGpx4
Gpx4(f/f)
Gpx4NIKO
Li.
SM
SC
CC
Li.
SM
SC
CC
rGpx4
B
DAPI
GFP
Gpx4
Merge
- TAM
+ TAM
C
Gpx4(f/f)
Gpx4NIKO
Gpx4
Actin
Gpx4 protein
1.2
1
0.8
0.6
0.4
0.2
0
*
Gpx4(f/f)
Gpx4NIKO
D
Gpx4(f/f)
Gpx4NIKO
ChAT
E
Nissl
F
Gpx4NIKO - TAM
Gpx4NIKO + TAM
GFP
G
Gpx4(f/f)
Gpx4NIKO
ChAT
Actin
Syn
PSD95
NeuN
Actin
H
Gpx4(f/f)
Gpx4NIKO
Level of protein
1.2
1
0.8
0.6
0.4
0.2
0
*
*
*
*
ChAT
Syn
PSD95
NeuN

Gpx4 in tissues from TAM-treated Gpx4NIKO mice. As shown in Fig. 2*A*, an amplicon derived from recombined *Gpx4* alleles (rGpx4) was obtained in spinal cord and cerebral cortex tissues but not in skeletal muscle or liver tissues of Gpx4NIKO mice, confirming the neuron-specific ablation of *Gpx4* in Gpx4NIKO mice (Fig. 2*A*). We next stained spinal cord sections from Gpx4NIKO mice without TAM treatment and Gpx4NIKO mice with TAM treatment (obtained on day 1 post-treatment) with an antibody against GPX4. As shown in Fig. 2*B*, spinal cord neurons from TAM-treated Gpx4NIKO mice showed reduced GPX4 immunofluorescence compared with those from control Gpx4NIKO mice without TAM treatment. We also compared GPX4 protein levels between TAM-treated Gpx4(f/f) mice and Gpx4NIKO mice on day 6 post treatment, and the results showed that Gpx4NIKO mice had a significantly reduced GPX4 protein level in spinal cord tissue (Fig. 2*C*). Together, these results indicated that TAM treatment led to ablation of *Gpx4* in spinal neurons of Gpx4NIKO mice.

To determine whether paralysis in TAM-treated Gpx4NIKO mice was a result of degeneration of motor neurons, we stained lumbar spinal cord sections from paralyzed Gpx4NIKO mice and control Gpx4(f/f) mice (on day 6 post-TAM treatment) with an antibody against choline acetyltransferase (ChAT), a motor neuron-specific protein. As shown in Fig. 2*D*, no intact ChAT-positive motor neurons could be observed in lumbar spinal cord from Gpx4NIKO mice. Consistent with the ChAT immunofluorescence data, spinal cords from Gpx4NIKO mice also had reduced Nissl-stained large neurons in the ventral horn region compared with Gpx4(f/f) mice (Fig. 2*E*), and spinal cords from Gpx4NIKO mice treated with TAM had reduced GFP-positive large neurons compared with control Gpx4NIKO mice without TAM treatment (Fig. 2*F*). Consistent with the immunofluorescence results, Gpx4NIKO mice also had a significantly lower level of ChAT protein than Gpx4(f/f) mice, as determined by Western blots (Fig. 2, *G* and *H*). We further compared levels of three other neural marker proteins (synaptophysin, a neuronal presynapse protein; PSD95, a neuronal postsynapse protein; and NeuN, a neuronal nuclear protein) between Gpx4NIKO mice and Gpx4(f/f) mice. As shown in Fig. 2, *G* and *H*, levels of synaptophysin, PSD95, and NeuN protein were decreased significantly in spinal cords of Gpx4NIKO mice. Together, these results indicated that the paralyzed Gpx4NIKO mice had a dramatic degeneration of motor neurons in the spinal cord.

No Overt Neurodegeneration in the Cerebral Cortex of the Paralyzed Gpx4NIKO Mice—Our results so far indicated that a robust degeneration of spinal motor neurons led to paralysis and muscle atrophy in TAM-treated Gpx4NIKO mice. Ablation of *Gpx4* also occurred in the cerebral cortex of TAM-treated Gpx4NIKO mice (Fig. 2*A*), so we wondered whether neurodegeneration occurred in this region of Gpx4NIKO mice as well. To this end, we compared levels of GPX4 protein and the three neural marker proteins levels in cerebral cortex tissues from paralyzed Gpx4NIKO mice and control Gpx4(f/f) mice (on day 6 post-TAM treatment). As expected, Gpx4NIKO mice had a decreased level of GPX4 protein compared with Gpx4(f/f) mice (Fig. 3, *A* and *B*). However, no decrease in synaptophysin, NeuN, and PSD95 levels was observed in Gpx4NIKO mice (Fig. 3, *A* and *B*). Therefore, despite the robust motor neuron degeneration in the spinal cord, no overt neurodegeneration occurred in the cerebral cortex of Gpx4NIKO mice.

The results therefore suggest that, unlike motor neurons in the spinal cord, other neurons, such as those from the cerebral cortex of adult animals, are relatively resistant to Gpx4 ablation. To test this, we further studied the effect of Gpx4 ablation in another neuron-inducible Gpx4 knockout mouse model: Gpx4(f/f);Camk2α-creERT mice. Gpx4(f/f);Camk2α-creERT mice were obtained by cross-breeding Gpx4(f/f) mice with a Camk2α-creERT transgenic mouse in which the expression of creERT is driven by a Camk2α promoter (14). Camk2α-positive neurons are rich in forebrain regions, so the Camk2α promoter-driven expression of creERT in Gpx4(f/f);Camk2α-creERT mice would allow us to study the effect of *Gpx4* ablation on neurons in brain regions such as the cerebral cortex and hippocampus (14). To this end, cohorts of Gpx4(f/f);Camk2α-creERT mice and control Gpx4(f/f) mice were subjected to TAM treatment. As shown in Fig. 3*C*, rGpx4 was detected in the cerebral cortex and hippocampus of Gpx4(f/f);Camk2α-creERT mice after TAM treatment but not in liver or skeletal muscle, thereby confirming neuron-specific ablation of *Gpx4* in Gpx4(f/f);Camk2α-creERT mice. We next compared levels of GPX4 and the neural marker proteins between Gpx4(f/f); Camk2a-creERT mice and Gpx4(f/f) mice 2 weeks post-TAM treatment. As shown in Fig. 3, *D* and *E*, although a decrease in GPX4 protein was evident, no decrease in the levels of synaptophysin, NeuN, and PSD95 proteins was observed in cortex tissues from Gpx4(f/f);Camk2α-creERT mice, indicating that *Gpx4* ablation did not result in overt neuron degeneration at this time point. Together, the results from Gpx4NIKO mice and Gpx4(f/f);Camk2α-creERT mice indicate that spinal motor neurons are selectively vulnerable to *Gpx4* deletion.

Motor Neuron Degeneration Induced by Gpx4 Ablation Was Characterized by Ferroptosis—GPX4 has recently been identified as a key inhibitor of ferroptosis (7). To determine whether ablation of *Gpx4* resulted in motor neuron death by ferroptosis, we first tried to detect apoptotic markers that have been reported to be absent in ferroptosis. Caspase-3 activation is a hallmark of apoptosis that does not occur in ferroptosis (6). To determine whether motor neuron degeneration induced by

FIGURE 2. **A dramatic degeneration of spinal cord motor neurons in the paralyzed Gpx4NIKO mice.** *A*, detection of the recombined *Gpx4* gene allele (rGpx4) by PCR only in nervous tissues from TAM-treated Gpx4NIKO mice. *SC*, spinal cord; *CC*, cerebral cortex; *SM*, skeletal muscle; *Li*, liver. *B*, spinal cord sections from control Gpx4NIKO mice without TAM treatment (− TAM) and TAM-treated Gpx4NIKO mice (+ TAM), showing reduced GPX4 immunofluorescence in spinal neurons of Gpx4NIKO mice. *C*, representative Western blots of GPX4 protein in spinal cord tissues and quantified GPX4 protein levels in spinal cord tissues ($n = 9$, male and female) for both groups. *, $p < 0.05$. *D*, lumbar spinal cord sections from Gpx4(f/f) mice and Gpx4NIKO mice on day 6 post-TAM treatment, showing ChAT-positive motor neurons. *E*, Nissl-stained lumbar spinal cord sections from Gpx4(f/f) mice and Gpx4NIKO mice. *F*, lumbar spinal cord sections from control Gpx4NIKO mice (− TAM) and Gpx4NIKO mice with TAM treatment (+ TAM), showing GFP-positive spinal cord neurons. *G*, representative Western blots showing levels of ChAT, synaptophysin (*Syn*), PSD95, and NeuN in spinal cord tissues from Gpx4NIKO mice and Gpx4(f/f) mice. *H*, quantified results of ChAT, Syn, PSD95, and NeuN levels in spinal cords from Gpx4NIKO mice and Gpx4(f/f) mice ($n = 9$, male and female). *, $p < 0.05$. *Scale bars* = 20 μm.

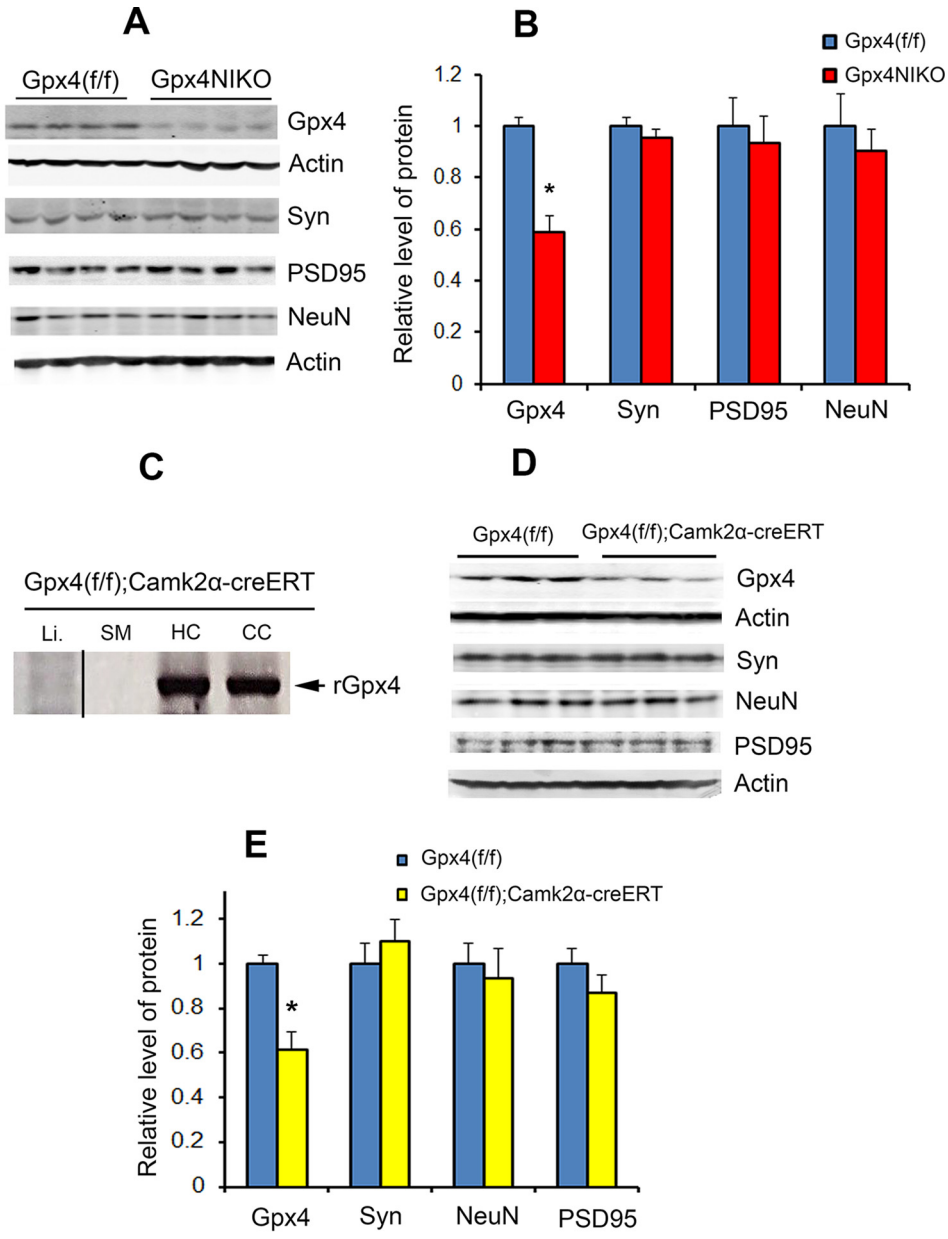

FIGURE 3. ***Gpx4* ablation resulted in no overt neurodegeneration in the cerebral cortex.** *A*, Western blots showing levels of GPX4, Syn, NeuN, and PSD95 in cortex tissues from Gpx4(f/f) mice and Gpx4NIKO mice on day 6 post TAM treatment ($n = 9$, male and female). *B*, quantified levels of GPX4, Syn, NeuN, and PSD95 in cortex tissues. *, $p < 0.05$. *C*, detection of rGpx4 by PCR only in nervous tissues from TAM-treated Gpx4(f/f);Camk2α-creERT mice. The image was assembled from different parts of a gel. *CC*, cerebral cortex; *HC*, hippocampus; *SM*, skeletal muscle; *Li*, liver. *D*, Western blots showing levels of GPX4, Syn, NeuN, and PSD95 in cortex tissues from Gpx4(f/f) mice and Gpx4(f/f);Camk2α-creERT mice 2 weeks post-TAM treatment. *E*, quantified levels of GPX4, Syn, NeuN, and PSD95 in cortex tissues from Gpx4(f/f) mice and Gpx4(f/f);Camk2α-creERT mice 2 weeks post-TAM treatment ($n = 3$, male and female). *, $p < 0.05$.

Gpx4 ablation was associated with caspase-3 activation, we measured cleavage of capaspase-3 in spinal cord obtained on day 3 by Western blots. As shown in Fig. 4*A*, no cleavage of caspase-3 was detected in spinal cord of Gpx4NIKO mice after TAM treatment. As shown in Fig. 4*B*, motor neurons from TAM-treated Gpx4NIKO mice were also negative for TUNEL staining, another marker of apoptosis.

We next tried to detect positive markers that have been reported to associate with ferroptosis. Activation of ERK signaling is a signature of ferroptosis (15). To investigate whether this marker was associated with motor neuron degeneration in Gpx4NIKO mice, we compared the levels of ERK phosphorylation in spinal cord of Gpx4(f/f) mice and Gpx4NIKO mice. As shown in the Fig. 4, *C* and *D*, spinal cord of Gpx4NIKO mice showed a marked increase in phospho-ERK1/2, indicating activation of ERK signaling.

Another difference between ferroptosis and apoptosis is how cellular contents are handled. Cells dying through apoptosis release a minimum amount of cytoplasmic contents, causing no inflammation (16). In contrast, cells dying through ferroptosis release soluble and lipid reactive oxygen species (17), which are predicted to result in elevated inflammation. To determine whether motor neuron degeneration in Gpx4NIKO mice resulted in inflammation, we stained spinal cord sections from Gpx4NIKO mice (on day 6 post-TAM treatment) with an antibody against GFAP, a marker of activated astrocytes, and with

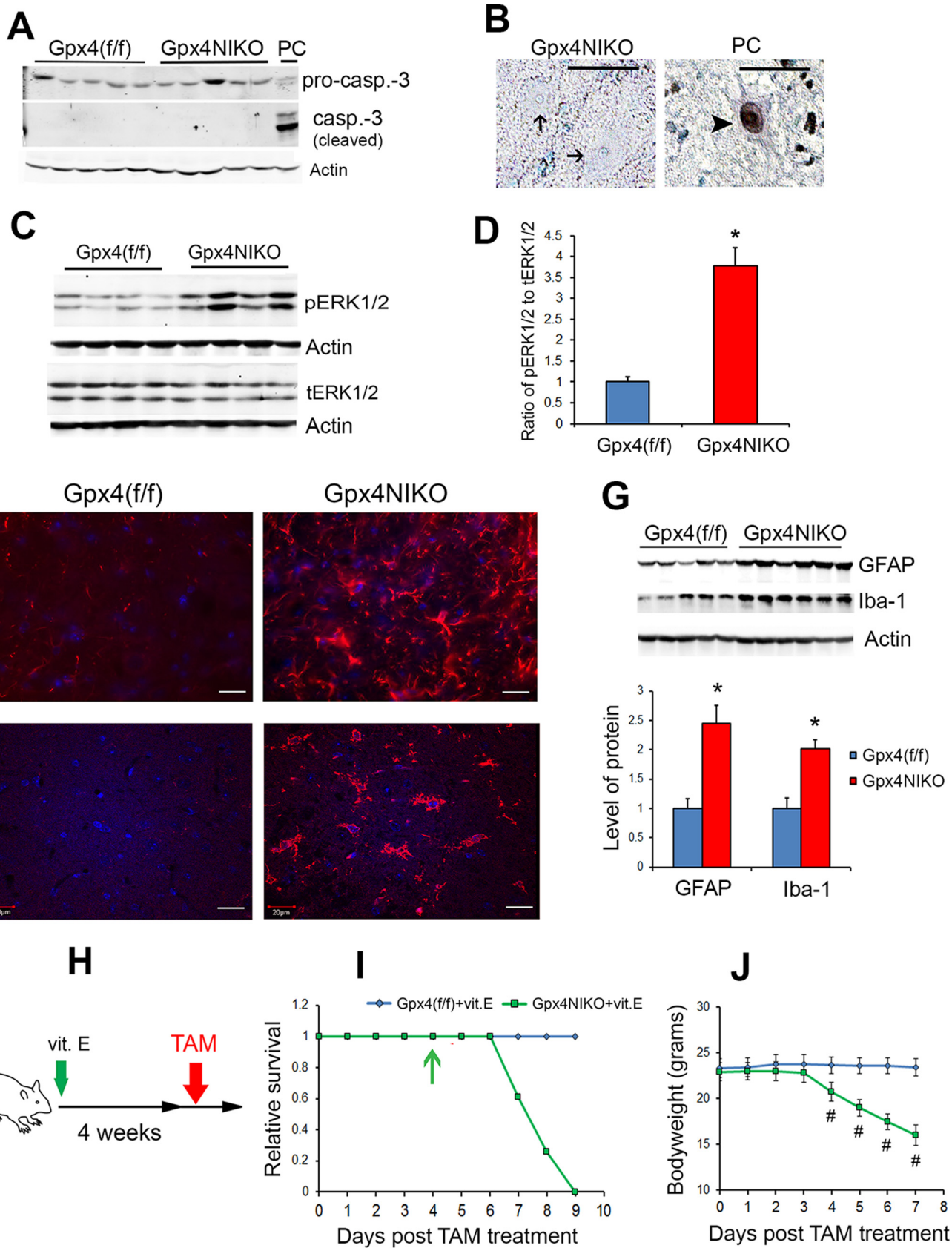
A
Gpx4(f/f)
Gpx4NIKO
PC
pro-casp.-3
casp.-3
(cleaved)
Actin
B
Gpx4NIKO
PC
C
Gpx4(f/f)
Gpx4NIKO
pERK1/2
Actin
tERK1/2
Actin
D
Ratio of pERK1/2 to tERK1/2
Gpx4(f/f)
Gpx4NIKO
E
Gpx4(f/f)
Gpx4NIKO
GFAP/DAPI
F
Iba-1/DAPI
G
Gpx4(f/f)
Gpx4NIKO
GFAP
Iba-1
Actin
Level of protein
GFAP
Iba-1
H
vit. E
TAM
4 weeks
I
Gpx4(f/f)+vit.E
Gpx4NIKO+vit.E
Relative survival
Days post TAM treatment
J
Bodyweight (grams)
Days post TAM treatment

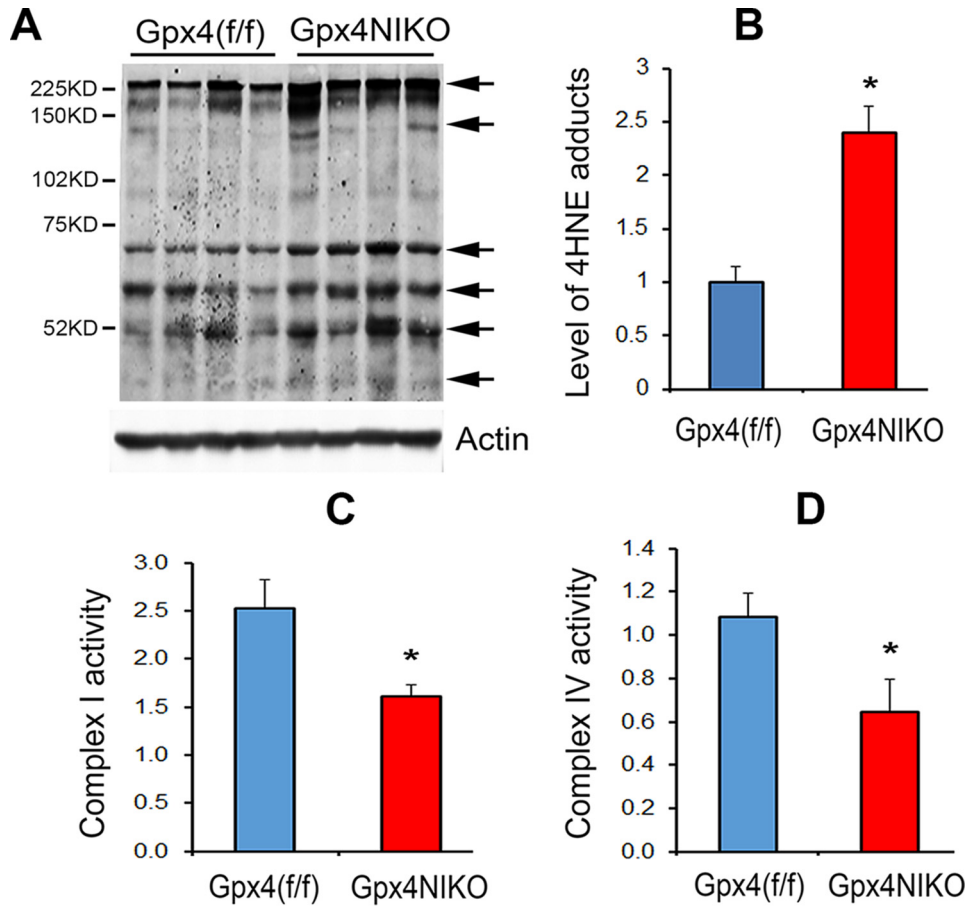

FIGURE 5. **Increased lipid peroxidation and mitochondrial dysfunction at onset of paralysis in TAM-treated Gpx4NIKO mice.** *A*, Western blots of spinal cord proteins probed with an anti-4-HNE antibody and then with an anti-actin antibody to control loading. *Arrows* indicate 4-HNE protein adducts. Tissues were obtained on day 3 post TAM treatment. *B*, quantified results of 4-HNE adducts ($n = 4$, male and female). *, $p < 0.05$. *C*, activity of electron transport chain complex I of spinal cord mitochondria on day 3. *, $p < 0.05$. *D*, activity of electron transport chain complex IV of spinal cord mitochondria on day 3 ($n = 5$). *, $p < 0.05$.

an antibody against Iba-1, a marker of activated microglia. As shown in Fig. 4*E*, spinal cords from Gpx4NIKO mice had significantly intensified staining for GFAP-positive astrocytes, indicating astrogliosis. Spinal cord sections from Gpx4NIKO mice also had an abundance of Iba-1-positive microglia (Fig. 4*F*). We further compared levels of GFAP and Iba-1 proteins between Gpx4(f/f) mice and Gpx4NIKO mice. Consistent with the immunofluorescence results, Gpx4NIKO mice showed significantly higher levels of GFAP protein and Iba-1 protein than Gpx4(f/f) mice (Fig. 4*G*). Therefore, the augmented inflammation in spinal cord of TAM-treated Gpx4NIKO mice was consistent with motor neurons dying via ferroptosis.

Vitamin E has also been shown to be a ferroptosis inhibitor (6). To further investigate the importance of ferroptosis in motor neuron degeneration induced by Gpx4 ablation, we assessed the effect of vitamin E on paralysis development in Gpx4NIKO mice. Cohorts of Gpx4NIKO mice and control Gpx4(f/f) mice were fed a vitamin E-enriched diet (1000 IU/kg) for 4 weeks before commencing TAM treatment (Fig. 4*H*). As shown in Fig. 4*I*, the onset of paralysis (stiffness of hind limbs) in vitamin E-fed Gpx4NIKO mice occurred on day 4 post-TAM treatment, and the significant loss of body weight from the previous day also started on day 4 (Fig. 1*J*). Compared with Gpx4NIKO mice on a standard chow diet, the onset of paralysis was delayed by 1 day in vitamin E-fed Gpx4NIKO mice. After onset of paralysis, vitamin E-fed Gpx4NIKO mice progressed to become paralyzed in the lower body and died within 9 days post-TAM treatment. Compared with Gpx4NIKO mice on a standard chow diet, the death of mice was also delayed by 1 day. The partial rescue results from the vitamin E supplement study

FIGURE 4. **Motor neuron degeneration in Gpx4NIKO mice exhibited features of ferroptosis.** *A*, Western blots showing spinal proteins probed with an antibody against pro-caspase 3 (*pro-casp.-3*) and activated caspase-3 (*casp.-3 (cleaved)*). Tissues were obtained at day 3 post TAM treatment. *PC*, positive control. *B*, spinal motor neurons from Gpx4NIKO mice on day 3 post-TAM treatment stained by TUNEL. *Arrows* indicate TUNEL-negative nuclei. *PC*, positive control (a motor neuron treated with nuclease); *arrowhead*, a TUNEL-positive nucleus. *C*, Western blots showing levels of phosphorylated ERK1/2 (*pERK1/2*) and total ERK1/2 (*tERK1/2*) on day 6 post-TAM treatment. *D*, quantified ratios of pERK1/2 to tERK1/2. *E*, lumbar spinal cord sections from Gpx4(f/f) mice and Gpx4NIKO mice on day 6 post-TAM treatment stained with an anti-GFAP antibody. *, $p < 0.05$. *F*, lumbar spinal cord sections from Gpx4(f/f) mice and Gpx4NIKO mice stained with an anti-Iba-1 antibody. *G*, Western blots showing levels of GFAP and Iba-1 in spinal cord tissues from Gpx4(f/f) mice and Gpx4NIKO mice (day 6) and quantified results of GFAP and Iba-1 levels ($n = 5$–6, male and female). *, $p < 0.05$. *H*, design of the vitamin E (*vit. E*) supplement study. *I*, survival curves of vitamin E-fed Gpx4NIKO mice (*Gpx4NIKO+vit.E*, $n = 23$, male and female) and Gpx4(f/f) mice (*Gpx4(f/f)+vit.E*, $n = 22$, male and female) after TAM treatment. The *arrow* indicates onset of paralysis. *J*, body weights of vitamin E-fed Gpx4NIKO mice and Gpx4(f/f) mice after TAM treatment. #, $p < 0.01$. *Scale bars* = 20 μm.

therefore provided further support for ferroptosis in motor neuron degeneration of Gpx4NIKO mice. Together, these results indicate that, consistent with the role of GPX4 as a ferroptosis inhibitor, motor neuron degeneration induced by Gpx4 ablation was characterized by ferroptosis.

Lipid Peroxidation and Mitochondrial Dysfunction at the Onset of Paralysis in TAM-treated Gpx4NIKO Mice—We further investigated how ablation of *Gpx4* might result in ferroptosis of motor neurons. Lipid reactive oxygen species are a signature of ferroptosis. GPX4 can reduce peroxides in complex lipids such as phospholipids, cholesterol, and cholesterol ester, thereby affording protection against lipid peroxidation (18). To determine whether ablation of Gpx4 resulted in increased lipid peroxidation, we compared 4-HNE adduct levels in spinal cord tissues from Gpx4(f/f) mice and Gpx4NIKO mice at the onset of paralysis (on day 3) by Western blots. As shown in Fig. 5, *A* and *B*, Gpx4NIKO mice had increased 4-HNE protein adducts, indicating elevated lipid peroxidation. Previous studies have indicated that GPX4 is important for mitochondrial protection (19). To determine whether *Gpx4* ablation induced mitochondrial damage in motor neurons of Gpx4NIKO mice, we compared the activities of electron transport chain complex I and complex IV of spinal cord mitochondria from Gpx4NIKO mice and Gpx4(f/f) mice. As shown in Fig. 5, *C* and *D*, spinal cord mitochondria from Gpx4NIKO mice had significantly decreased activities of both electron transport chain complex I and complex IV. Therefore, increased lipid peroxidation and reduced mitochondrial function might be important in ferroptosis of motor neurons induced by *Gpx4* ablation.

Discussion

GPX4 is a selenoprotein glutathione peroxidase with pleotropic functions in different cell types. In this study, to investigate the importance of GPX4 in the neuron health of adult animals, we generated a neural conditional *Gpx4* knockout mouse model, *i.e.* the Gpx4NIKO mouse, in which ablation of *Gpx4* in neurons can be achieved by TAM treatment. We showed that TAM treatment to ablate *Gpx4* induced a striking paralysis phenotype in adult Gpx4NIKO mice. The mice became paralyzed rapidly, exhibited severe muscle atrophy, and died within 8 days. The paralysis in Gpx4NIKO mice was driven by a marked degeneration of motor neurons in the spinal cord. Our results therefore indicate that *Gpx4* is an essential gene for motor neuron health and survival in adult animals.

GPX4 has been shown previously to regulate apoptosis (2–4), because GPX4 can decrease the level of cardiolipin oxidation in the mitochondrial inner membrane, thereby suppressing cytochrome *c* dissociation from the mitochondrial inner membrane and subsequent release to the cytoplasm to induce apoptosis. Recently, GPX4 has also been shown to be a key inhibitor of ferroptosis (7). Interestingly, motor neuron degeneration induced by *Gpx4* ablation appeared to occur via ferroptosis, because ferroptosis features such as lack of caspase-3 activation, lack of TUNEL staining, activation of ERKs, and augmented spinal inflammation were observed. In addition, we showed that supplementation with vitamin E, also a ferroptosis inhibitor, delayed the onset of paralysis and death in Gpx4NIKO mice. Our results further implicated increased lipid peroxidation and mitochondrial dysfunction in ferroptosis of motor neuron induced by *Gpx4* ablation. At present, the selectivity of GPX4 in inhibiting apoptosis or ferroptosis is unclear. However, it is possible that the importance of GPX4 as an apoptosis or ferroptosis inhibitor may be dependent on the cell type and stress conditions. For instance, if a stress elicits lipid damage to trigger primarily apoptosis or ferroptosis in a certain cell type, then the respective role of apoptosis or ferroptosis inhibition of GPX4 will manifest. The reason why ablation of *Gpx4* in motor neurons induces ferroptosis is unclear. Whether this is due to a cellular environment that is conducive to ferroptosis remains to be determined.

Interestingly, no overt neuron degeneration in the cerebral cortex was observed in paralyzed Gpx4NIKO mice, even though ablation of GPX4 also occurred in neurons of this region. In addition, no overt neurodegeneration was observed in the cerebral cortex of Gpx4(f/f);Camk2α-creERT mice 2 weeks post-TAM treatment to ablate *Gpx4*. We have reported previously that ablation of *Gpx4* in adult mice using Rosa26-creERT resulted in the death of mice with neuron degeneration in the brain. The Rosa26 promoter is a ubiquitous promoter, so ablation of *Gpx4* occurred in many cell types when using Rosa26-cerERT. Therefore, the loss of neurons in the brain of mice with *Gpx4* ablation by Rosa26-cerERT could be due to a systemic effect and/or a combined effect of ablation of *Gpx4* in both neurons and glia cells.

Our results in this study suggest that ferroptosis inhibition is particularly important for motor neurons. Motor neuron degeneration underlies motor neuron degenerative diseases such as amyotrophic lateral sclerosis (20). The dying motor neurons have been reported in some studies to exhibit features of apoptosis; however, non-apoptotic features in the degenerative motor neurons have been noted in other reports (21–24). Therefore, the overall mechanism of neurodegeneration in motor neuron degenerative diseases is still not completely known and may involve multiple types of programmed cell death pathways. In light of our findings, further research to investigate whether ferroptosis is a mechanism important in motor neuron-degenerative diseases and whether GPX4 expression and/or activity is compromised in diseases such as amyotrophic lateral sclerosis are warranted.

Author Contributions—C. L., R. N., and W. S. H. performed the experiments. Q. R. designed the experiments and wrote the manuscript.

Acknowledgments—We thank Shuko Lee for assistance with statistical analysis.

References

1. Brigelius-Flohé, R. (1999) Tissue-specific functions of individual glutathione peroxidases. *Free Radic. Biol. Med.* **27,** 951–965
2. Imai, H., and Nakagawa, Y. (2003) Biological significance of phospholipid hydroperoxide glutathione peroxidase (PHGPx, GPx4) in mammalian cells. *Free Radic. Biol. Med.* **34,** 145–169
3. Ran, Q., Van Remmen, H., Gu, M., Qi, W., Roberts, L. J., 2nd, Prolla, T., and Richardson, A. (2003) Embryonic fibroblasts from Gpx4$^{+/-}$ mice: a novel model for studying the role of membrane peroxidation in biological processes. *Free Radic. Biol. Med.* **35,** 1101–1109

4. Ran, Q., Liang, H., Gu, M., Qi, W., Walter, C. A., Roberts, L. J., 2nd, Herman, B., Richardson, A., and Van Remmen, H. (2004) Transgenic mice overexpressing glutathione peroxidase 4 are protected against oxidative stress-induced apoptosis. *J. Biol. Chem.* **279,** 55137–55146
5. Yang, W. S., and Stockwell, B. R. (2008) Synthetic lethal screening identifies compounds activating iron-dependent, nonapoptotic cell death in oncogenic-RAS-harboring cancer cells. *Chem. Biol.* **15,** 234–245
6. Dixon, S. J., Lemberg, K. M., Lamprecht, M. R., Skouta, R., Zaitsev, E. M., Gleason, C. E., Patel, D. N., Bauer, A. J., Cantley, A. M., Yang, W. S., *et al.* (2012) Ferroptosis: an iron-dependent form of nonapoptotic cell death. *Cell* **149,** 1060–1072
7. Yang, W. S., SriRamaratnam, R., Welsch, M. E., Shimada, K., Skouta, R., Viswanathan, V. S., Cheah, J. H., Clemons, P. A., Shamji, A. F., Clish, C. B., Brown, L. M., Girotti, A. W., Cornish, V. W., Schreiber, S. L., and Stockwell, B. R. (2014) Regulation of ferroptotic cancer cell death by GPX4. *Cell* **156,** 317–331
8. Yant, L. J., Ran, Q., Rao, L., Van Remmen, H., Shibatani, T., Belter, J. G., Motta, L., Richardson, A., and Prolla, T. A. (2003) The selenoprotein GPX4 is essential for mouse development and protects from radiation and oxidative damage insults. *Free Radic. Biol. Med.* **34,** 496–502
9. Imai, H., Hirao, F., Sakamoto, T., Sekine, K., Mizukura, Y., Saito, M., Kitamoto, T., Hayasaka, M., Hanaoka, K., and Nakagawa, Y. (2003) Early embryonic lethality caused by targeted disruption of the mouse PHGPx gene. *Biochem. Biophys. Res. Commun.* **305,** 278–286
10. Yoo, S. E., Chen, L., Na, R., Liu, Y., Rios, C., Van Remmen, H., Richardson, A., and Ran, Q. (2012) Gpx4 ablation in adult mice results in a lethal phenotype accompanied by neuronal loss in brain. *Free Radic. Biol. Med.* **52,** 1820–1827
11. Chen, L., Na, R., and Ran, Q. (2014) Enhanced defense against mitochondrial hydrogen peroxide attenuates age-associated cognition decline. *Neurobiol. Aging* **35,** 2552–2561
12. Young, P., Qiu, L., Wang, D., Zhao, S., Gross, J., and Feng, G. (2008) Single-neuron labeling with inducible Cre-mediated knockout in transgenic mice. *Nat. Neurosci.* **11,** 721–728
13. Heimer-McGinn, V., and Young, P. (2011) Efficient inducible Pan-neuronal cre-mediated recombination in SLICK-H transgenic mice. *Genesis* **49,** 942–949
14. Madisen, L., Zwingman, T. A., Sunkin, S. M., Oh, S. W., Zariwala, H. A., Gu, H., Ng, L. L., Palmiter, R. D., Hawrylycz, M. J., Jones, A. R., Lein, E. S., and Zeng, H. (2010) A robust and high-throughput Cre reporting and characterization system for the whole mouse brain. *Nat. Neurosci.* **13,** 133–140
15. Yagoda, N., von Rechenberg, M., Zaganjor, E., Bauer, A. J., Yang, W. S., Fridman, D. J., Wolpaw, A. J., Smukste, I., Peltier, J. M., Boniface, J. J., Smith, R., Lessnick, S. L., Sahasrabudhe, S., and Stockwell, B. R. (2007) RAS-RAF-MEK-dependent oxidative cell death involving voltage-dependent anion channels. *Nature* **447,** 864–868
16. Elmore, S. (2007) Apoptosis: a review of programmed cell death. *Toxicol. Pathol.* **35,** 495–516
17. Dixon, S. J., and Stockwell, B. R. (2014) The role of iron and reactive oxygen species in cell death. *Nat. Chem. Biol.* **10,** 9–17
18. Girotti, A. W. (1998) Lipid hydroperoxide generation, turnover, and effector action in biological systems. *J. Lipid Res.* **39,** 1529–1542
19. Liang, H., Van Remmen, H., Frohlich, V., Lechleiter, J., Richardson, A., and Ran, Q. (2007) Gpx4 protects mitochondrial ATP generation against oxidative damage. *Biochem. Biophys. Res. Commun.* **356,** 893–898
20. Kiernan, M. C., Vucic, S., Cheah, B. C., Turner, M. R., Eisen, A., Hardiman, O., Burrell, J. R., and Zoing, M. C. (2011) Amyotrophic lateral sclerosis. *Lancet* **377,** 942–955
21. Guegan, C., and Przedborski, S. (2003) Programmed cell death in amyotrophic lateral sclerosis. *J. Clin. Invest.* **111,** 153–161
22. Sathasivam, S., and Shaw, P. J. (2005) Apoptosis in amyotrophic lateral sclerosis: what is the evidence? *Lancet Neurol.* **4,** 500–509
23. Tomik, B., Adamek, D., Pierzchalski, P., Banares, S., Duda, A., Partyka, D., Pawlik, W., Kaluza, J., Krajewski, S., and Szczudlik, A. (2005) Does apoptosis occur in amyotrophic lateral sclerosis? TUNEL experience from human amyotrophic lateral sclerosis (ALS) tissues. *Folia Neuropathol.* **43,** 75–80
24. Yamazaki, M., Esumi, E., and Nakano, I. (2005) Is motoneuronal cell death in amyotrophic lateral sclerosis apoptosis? *Neuropathology* **25,** 381–387